SUPPLEMENTARY INFORMATION

Chiantia S. and E. London, "Acyl chain length and saturation modulate interleaflet coupling in asymmetric bilayers: effects on dynamics and structural order"

MATERIALS AND METHODS

Chemicals

1,2-dioleoyl-*sn*-glycero-3-phosphocholine (DOPC), 1-palmitoyl-2-oleoyl-*sn*-glycero-3-phosphocholine (POPC), 1-stearoyl-2-oleoyl-*sn*-glycero-3-phosphocholine (SOPC), 1-oleoyl-2-myristoyl-*sn*-glycero-3-phosphocholine (OMPC), sphingomyelin from porcine brain (bSM) or bovine milk (mSM), 1,2-dioleoyl-*sn*-glycero-3-phosphoethanolamine-N-(7-nitro-2-1,3-benzoxadiazol-4-yl) (NBD-DOPE) and 1,2- dihexadecanoyl -*sn*-glycero-3-phosphoethanolamine-N-(7-nitro-2-1,3-benzoxadiazol-4-yl) (NBD-DPPE) were purchased from Avanti Polar Lipids (Alabaster, AL). 1-(4-Trimethylammoniumphenyl)-6-phenyl-1,3,5-hexatriene *p*-toluenesulfonate (TMA-DPH) was from Invitrogen (Eugene, OR). Trehalose dihydrate, methyl-β-cyclodextrin (mβCD) and sodium dithionite were from Sigma-Aldrich (St. Louis, MO). Sepharose CL-4B and CL-2B were purchased from Amersham Biosciences (Piscataway, NJ). Sephacryl S-300 was from Pharmacia Biotech (now GE Healthcare), Piscataway, NJ. Phosphate buffered saline (PBS, 10 mM sodium phosphate, 150 mM sodium chloride) 1X pH 7.4 was from Bio-Rad, Hercules, CA. TRIS buffer was purchased from Roche Diagnostics (Indianapolis, IN). The conjugation of the Nile Red fluorophore with an anchor group to obtain NR12S was performed as previously described (1) and was a gift of A. Klymchenko (Université de Strasbourg, France). Atto647-acyl chain-labeled sphingomyelin (Atto-SM) (described in (2)) was a gift of P. Schwille (MPI Martinsried, Germany).

Preparation of the asymmetric GUVs

Symmetric and asymmetric GUVs were formed in ~70-100 mM trehalose as previously described (3), with only a few modifications to the protocol. For the asymmetric GUVs, the donor solution containing the lipid to be exchanged into the outer leaflet of the symmetric GUVs was prepared using a 16 mM SM (bSM or mSM) multilamellar vesicle (MLV) suspension in water. Before adding the mβCD (final concentration 71 mM from a 355 mM stock solution in water), the MLVs were centrifugated (10000g, 5 minutes, 23°C) and the supernatant was discarded. After a 2 h incubation at 55°C with mβCD, a centrifugation step to remove the residual SM MLVs was carried out at 4°C for 30 min at 400000g. The osmolarity of the donor solution was, at this step, between 100 and 120 mOsm/Kg (measured with a Micro-Osmometer 210, Advanced Instruments, Norwood, MA). For sake of simplicity, we assumed the mβCD to have a nominal concentration of 70 mM. The symmetric GUVs containing NBD-DOPE in both leaflets (0.01-0.03 mol% for FCS or 1 mol% for lifetime imaging), were then incubated for 30 min with the donor solution (mβCD concentration usually ~40-60 mM after dilution with water) to exchange the donor SM with outer leaflet PC, and then washed with 1 mL of the trehalose solution in which the vesicles were prepared. As discussed in (3), the higher the mβCD (and SM) concentration during the exchange, the higher the amount of SM delivered to the outer leaflet and the lower the final yield of asymmetric GUVs.

In order to quench permanently the NBD-DOPE in the outer leaflet of the now asymmetric GUVs, we washed the sample chamber with 1 mL sodium dithionite (0.5 mg/mL prepared from a 50 mg/mL fresh stock solution in TRIS buffer 293 mM pH 10) in trehalose

solution (ca. 90% of the original sugar concentration, in order to balance the osmolarity increase caused by sodium dithionite and TRIS). This step lasted 90 s. Thereafter, the sample was washed sequentially with: 1 mL trehalose solution, 1 mL trehalose solution containing 3 μL of a 14.3 μM stock of Atto-SM in ethanol and, again, 1 mL of trehalose solution. All the washing steps, starting with the donor solution for the lipid exchange, were performed keeping the osmolarity inside and outside the GUVs equal. The vesicles thus obtained contained, in the inner leaflet, the lipid with which the GUVs were initially prepared, while the outer leaflet contained a mix of the same lipid as in the inner leaflet with varying amounts of SM, depending mainly on mβCD concentration. It should be noted that the final concentration of SM in the outer leaflet is significantly heterogeneous from vesicle-to-vesicle, probably because some GUVs are surrounded by other vesicles, and hence not fully exposed to the donor solution. For each examined lipid composition, we prepared at least two independent preparations using, in general, two different mβCD concentrations for the lipid exchange (typically 50 and 57 mM) in order to obtain a large range of SM concentrations in the outer leaflet.

The lipid composition of asymmetric GUVs is identified in the text by writing the name of the lipid in the inner leaflet (followed by "i/") and the name of the lipid exchanged into the outer leaflet (followed by "o"). For example, GUVs with DOPC in the inner leaflet and bSM exchanged into the outer leaflet are referred to as DOPCi/bSMo GUVs. For this specific composition, we obtained asymmetric GUVs with an amount of bSM in the outer leaflet up to ~55mol%, as judged by lateral diffusion vs. that in symmetric GUV with different amounts SM (3). (In extreme cases, GUV surrounded by other GUVs failed to exchange in any significant amount of SM.)

Each vesicle was labeled both with NBD-DOPE in the inner leaflet and Atto-SM in the outer leaflet. The concentration of Atto-SM in the outer leaflet exhibited a degree of variation depending on the exposure of the vesicle to the washing steps.

Preparation of the asymmetric SUVs

Symmetric and asymmetric SUVs were formed as previously described (4) (see fig.1A therein). For asymmetric SUVs, the donor mβCD-SM solution contained 500 μL 16 mM SM MLVs in PBS and 105 μL 355 mM mβCD in water (thus obtaining 605 μL 13.2 mM SM and 61.6 mM mβCD). After a 2 h incubation at 55°C, the donor solution was mixed with 500 μL of sonicated SUVs (4mM lipid) in PBS for 30 min at the same temperature. Separation of multilamellar SM vesicles from the asymmetric SUV was performed using either a Sepharose CL-2B or CL-4B gel filtration column equilibrated and eluted with PBS. The lipid composition of asymmetric SUVs is identified by writing the name of the lipid in the inner leaflet (followed by "i/") and the name of the lipid exchanged into the outer leaflet (followed by "o"). For example, SUVs with DOPC in the inner leaflet and bSM in the outer leaflet are referred to as DOPCi/bSMo SUVs. Note that, in the case of asymmetric SUVs and differently from GUVs, the outer leaflet usually contains almost exclusively the exchanged lipid (for the example above: bSM), due to the high degree of exchange of outer leaflet lipids (4).

In order to label the outer leaflet of the asymmetric SUVs with TMA-DPH, the selected fraction with the highest SUV concentration from the Sepharose gel filtration (ca. 200 μM lipids) was divided in two samples, diluted to ca. 100 μM lipid concentration with PBS and mixed with a small aliquot (ca. 1 μL) of a concentrated ethanol stock solution of TMA-DPH to obtain a final molar concentration of 0.1-0.2 mol% compared to the lipids. In order to label the inner leaflet of asymmetric SUVs with TMA-DPH, we prepared vesicles initially containing (in both leaflets) 0.7-1 mol% TMA-DPH. After the above-mentioned procedure to produce the asymmetric SUVs, we collected one 1 mL fraction with the highest SUV concentration (ca. 200 μM). To remove any residual TMA-DPH left in the outer leaflet

(a large fraction of which was likely to already have been removed during the exchange procedure), we followed the protocol described previously (5), using 5 mM mβCD and a quick gel filtration on a ca. 5 cm long Sephacryl S-300 column, eluting with PBS. The two fractions with the highest vesicle concentration (66-100 μM) from the S-300 column were further analyzed. The amount of TMA-DPH in the inner leaflet at this step was such that the measured fluorescent intensity was similar to that measured in a sample with similar lipid concentration and labeled with 0.2 mol% TMA-DPH in the outer leaflet. TMA-DPH anisotropy at 23°C was calculated after background subtraction using the experimental setup described in ref. (5).

In order to label the inner leaflet of asymmetric SUVs with NBD-DPPE (or NR12S), we prepared the asymmetric vesicles containing 1 mol% NBD-DPPE (or 0.6 mol% NR12S) distributed in both leaflets, similarly to how described for TMA-DPH containing samples. The selected fraction with the highest SUV concentration from the Sepharose gel filtration (ca. 200 μM lipids) was divided in two samples, diluted to ca. 100 μM lipid concentration with PBS, and the residual fluorescent probe in the outer leaflet was quenched by adding to each sample 10 μL of a fresh stock solution containing 50 mg/mL sodium dithionite in TRIS pH 10 and waiting ca. 2 minutes before measuring the fluorescence signal. Fluorescence lifetime of NBD-DPPE was measured as described in the following paragraph. The emission wavelength of NR12S in the inner leaflet was measured using the experimental setup described in ref. (5).

Fluorescence lifetime measurements in asymmetric and symmetric SUVs

Fluorescence lifetime decays at 23°C were obtained by exciting NBD-DPPE in SUVs using a 470 nm pulsed diode laser (PDL 200, 4 MHz repetition rate, PicoQuant, Berlin, Germany). Depending upon the relative intensity measured in the different samples, slits providing bandwidths of 1 or 0.5 mm were employed. The fluorescence light passing through a monocromator set on 520 nm was detected by a PMA-182 photomultiplier based on the Hamamatsu H5783 photosensor modules (PicoQuant). The instrumental response function (IRF) for reconvolution was calculated by measuring the scattered light with the monocromator set at 470 nm. The photon count rate was on the order of $6-8\cdot10^4$ counts/s for the probes and $1\text{-}4\cdot10^3$ counts/s for IRF acquisition. For each sample, we acquired 3 decay histograms with peak values of 10000 events. A typical measurement to collect a single histogram lasted ca. 1 minute. Data analysis was conducted using a global nonlinear least-squares iterative procedure on the 3 histograms, and the goodness of fitting was judged by the distribution of the residuals and the χ^2 value. Fluorescence decays were analyzed with FluoFit (PicoQuant) using a two-component exponential model.

Fluorescence lifetime imaging of asymmetric and symmetric GUVs

Images (256 x 256 pixels) were taken by confocal laser scanning microscopy as described previously (6) using an inverted Fluoview 1000 microscope (Olympus, Tokyo, Japan) and a 60x (numerical aperture 1.2) water-immersion objective at 23°C. The detection unit was a commercial FLIM upgrade kit (PicoQuant). NBD-DPPE was excited via a pulsed diode laser (pulse width: 60 ps; pulse frequency: 10 MHz) with a wavelength of 468 nm. Emission was recorded using a 500-600 nm band-pass filter. Single photons were registered with an avalanche photo diode. Each image acquisition lasted 100 s and the average photon count rate was 10^5counts/s. The images were color-coded according to a fast, but approximate, algorithm providing one average lifetime for the arrival time of the photons binned in each pixel. For a more accurate determination of single fluorescence lifetimes components, we restricted the analysis on the GUVs (i.e. manually excluding bright regions not associated with membranes,

aggregates or leaky vesicles, such as those in fig. S2 D), and a fluorescence decay curve was generated. The IRF for reconvolution was calculated by measuring the fluorescence signal originating from a drop of KI saturated erythrosine B solution on a glass coverslip (7). Using a non-linear least squares iterative fitting procedure, fluorescence decay curves were fitted as a sum of two exponential terms to obtain the fluorescence lifetimes of the NBD-group. Typically, two lifetimes already provided adequate fitting (see Results section). Quality of fits was judged by the distribution of the residuals and the χ^2 value.

FCS measurements in asymmetric and symmetric GUVs

Single-spot FCS measurements were performed either on a laser scanning microscope (LSM) Zeiss ConfoCor3 (Carl Zeiss, Jena, Germany) using a 40X NA 1.2 UV-VIS C Apochromat water-immersion objective or on inverted Fluoview 1000 microscope (Olympus) with FLIM upgrade kit (PicoQuant) using a 60x NA 1.2 water-immersion objective. The sample was excited either by a 488 nm (green channel, NBD-DOPE) or a 633 nm (red channel, Atto-SM) laser. The fluorescence was then collected through either a 505-610 nm band pass filter for NBD-DOPE and a 70 μm pinhole or a 655 nm long pass filter for Atto-SM and a 80 μm pinhole. Unless differently noted, samples were usually produced at least in duplicates (i.e. two independent preparations). In each preparation, we typically analyzed 10 GUVs in different locations of the observation chamber. For each GUV, we acquired 6 to 10 independent fluorescence intensity tracks (corresponding to an equal amount of FCS curves), each 10 to 6 seconds long respectively, on top of the vesicle both for NBD-DOPE and Atto-SM. The FCS correlation curves were calculated using the Zeiss ConfoCor3 software and fitted using a nonlinear least squares algorithm to single-component 2D diffusion model. Triplet-state blinking contribution was not taken into account, due to the long diffusion times measured in the lipid bilayer (≥1ms). Diffusion times (both for NBD-DOPE and Atto-SM) in asymmetric GUVs were then compared to a calibration sample prepared daily. The calibration sample consisted of symmetric GUVs with a composition equal to that of the inner leaflet of the asymmetric sample (e.g. pure DOPC if dealing with DOPCi/SMo asymmetric samples) labeled with NBD-DOPE in the inner leaflet and Atto-SM in the outer leaflet. The calibration sample was subjected to the same labeling procedures (e.g. incubation with sodium dithionite) used to produce asymmetric GUVs. The diffusion times measured in asymmetric GUVs were then compared to the average diffusion times measured in the calibration sample, for the red channel and the green channel separately, to calculate the relative diffusion coefficients of each asymmetric GUV. Typical diffusion times for the control sample (e.g. DOPC) were 1.4 ms for Atto-SM and 0.9 ms for NBD-DOPE. A relative diffusion coefficient of, for example, 50% would therefore indicate a diffusion time of 2.8 ms (1.8 ms) for Atto-SM (NBD-DOPE). All measurements were performed at room temperature (i.e. 23°C). GUVs with relative outer leaflet diffusion >80% were not considered for quantitative analysis.

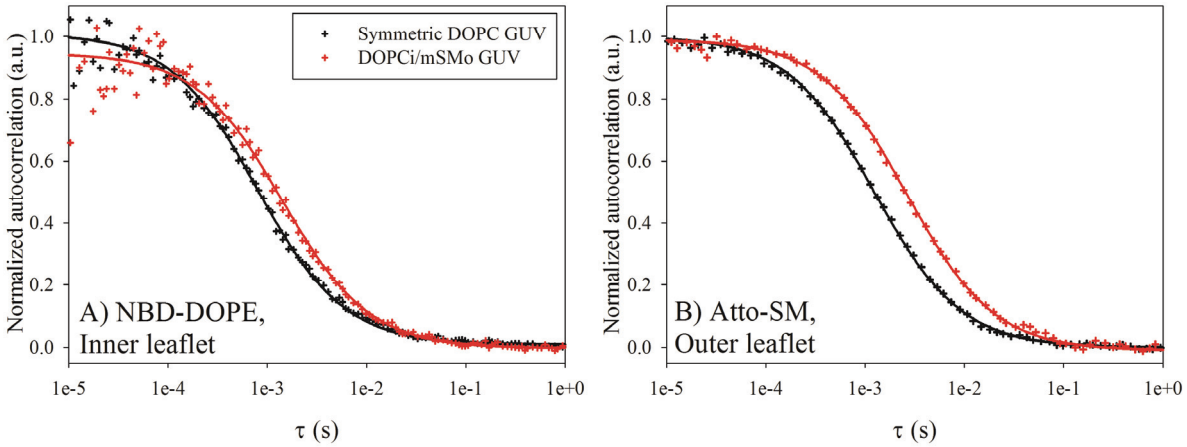

FIGURE S1. Representative normalized FCS autocorrelation curves for symmetric and asymmetric GUVs. A) Typical normalized autocorrelation curves measured for NBD-DOPE diffusing in the inner leaflet of a symmetric DOPC GUV (black) or an asymmetric DOPCi/mSMo GUV (red). B) Typical normalized autocorrelation curves measured for Atto-SM diffusing in the outer leaflet of the same GUVs referred to in panel A). Black data points represent the autocorrelation for Atto-SM in the symmetric DOPC GUV and red data points represent the autocorrelation for Atto-SM in the asymmetric DOPCi/mSMo GUV. Each curve is the average of ~6-10 autocorrelation curves obtained in a single GUV. Autocorrelation curves for NBD-DOPE and Atto-SM were measured sequentially in the same GUV. The solid lines are the best fit of the data to a single-component 2D diffusion model.

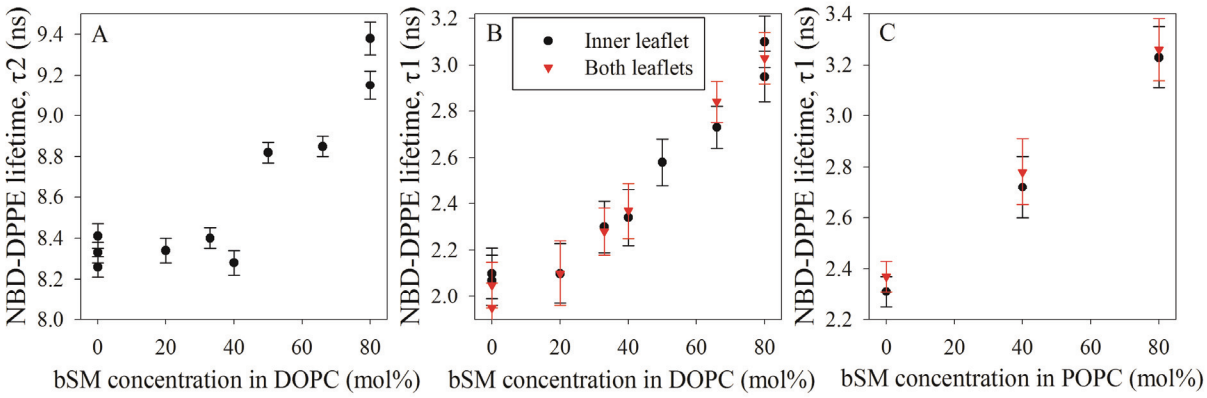

FIGURE S2. Calibration measurements for the fluorescence lifetime of NBD-DPPE in symmetric PC/bSM SUVs at 23°C. Fluorescence lifetime decays were recorded as described in the Materials and Methods section and analyzed using a two-component exponential decay model. A) Slow component τ2 of inner leaflet NBD-DPPE fluorescence lifetime decay as a function of bSM concentration in DOPC SUVs. B) Fast component τ1 of NBD-DPPE fluorescence lifetime decay as a function of bSM concentration in DOPC SUVs. C) Fast component τ1 of NBD-DPPE fluorescence lifetime decay as a function of bSM concentration in POPC SUVs. Values recorded with the fluorescent probe in both leaflets (red triangles) or restricted just to the inner leaflet (black circles) are undistinguishable within experimental uncertainty. All the reported values were obtained from 4 measurements in 2 independent preparations. Error bars represent standard deviations.

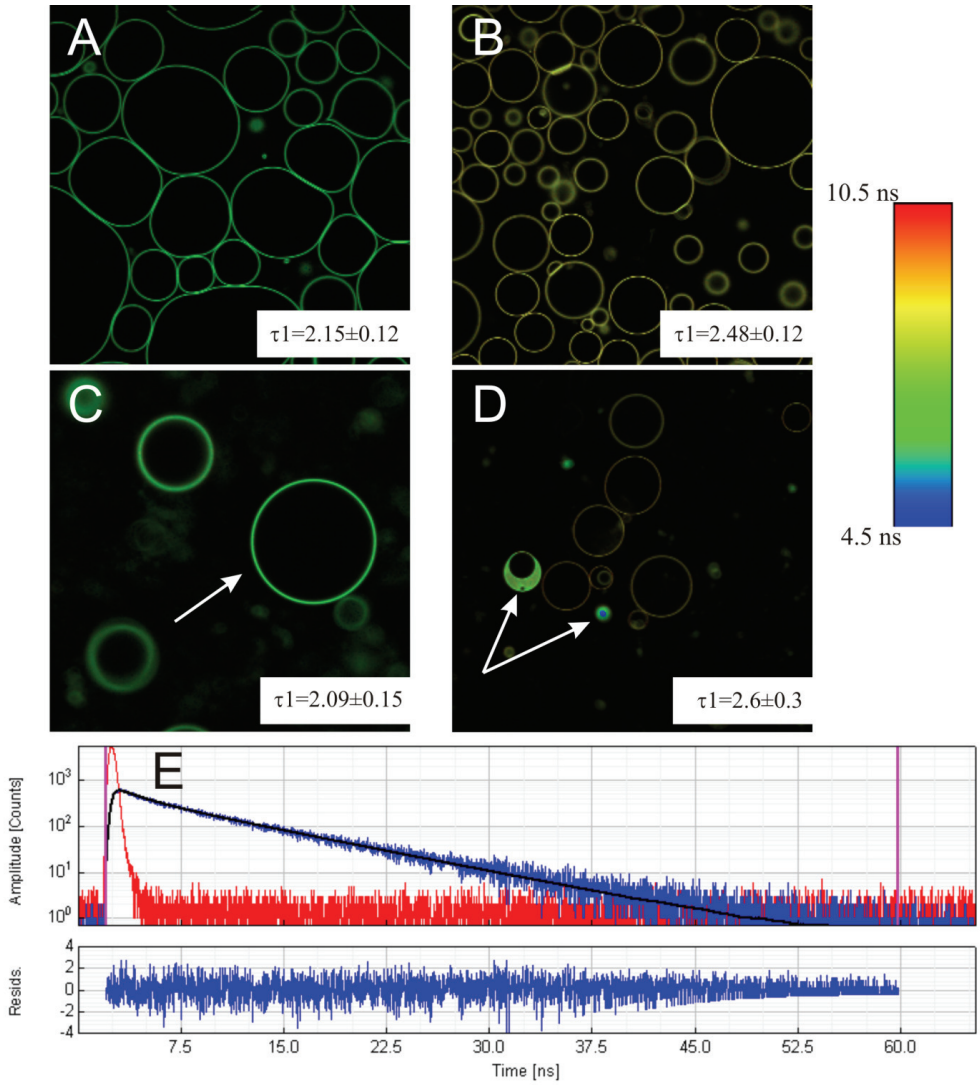

FIGURE S3. Probing the state of the inner leaflet using fluorescence lifetime imaging in asymmetric GUVs. Representative color-coded images of average fluorescence lifetime of NBD-DPPE in symmetric GUVs made of DOPC (panel A), POPC (panel B) or in asymmetric GUVs with composition DOPCi/bSMo (panel C) and POPCi/bSMo (panel D). The dye was distributed equally between the two leaflets in symmetric vesicles (A and B), while it was restricted to the inner leaflet for the asymmetric vesicles (C and D). Each image is 211.6 µm x 211.6 µm. The arrows in panel D indicates aggregates or solubilized dye that were typically excluded from further analysis. A more quantitative analysis of the NBD-DPPE lifetime was obtained by calculating lifetime histograms for all the photons collected during the image acquisition (ca. 100 s). Panel E shows an example of such a histogram relative to the photons collected from the GUV indicated by the arrow in panel C. The blue curve indicates the experimental data which we fit to a 2-component exponential decay (solid curve). The red curve is the IRF for the detection system which was used for a deconvolution-based fit of the data. The fast component τ1 of the lifetime decay so obtained was averaged over at least 6 images from duplicate samples and are reported in the lower right corner of panel A through panel D (slow component τ2 is omitted, see main text).

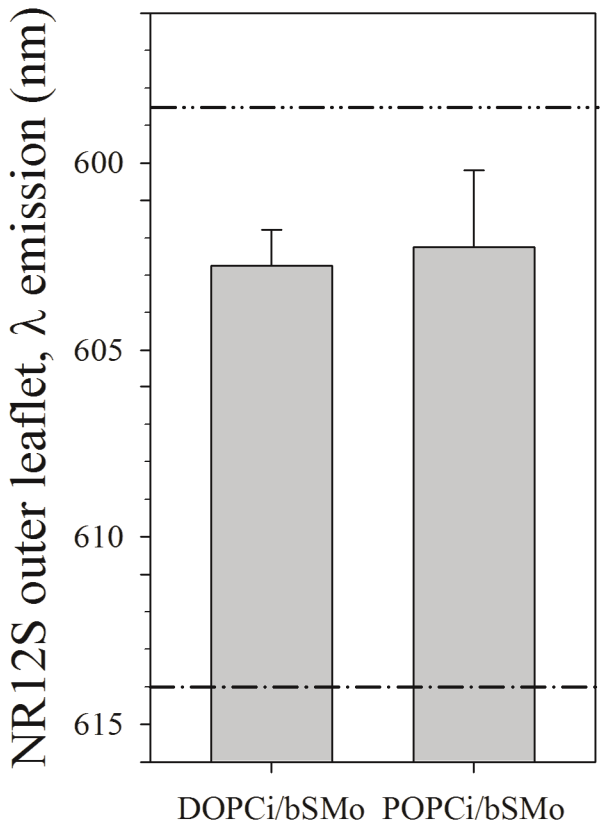

FIGURE S4. Outer leaflet NR12S fluorescence emission wavelength in asymmetric SUVs. Maximum emission wavelength of NR12S in the outer leaflet of asymmetric SUVs with varying compositions. All the reported values were obtained from 4 measurements in 2 independent preparations. Error bars represent standard deviations. Lines are reference values for symmetric DOPC outer leaflet (dash-dot), and DOPC:bSM 1:4 outer leaflet (dash-dot-dot). Reference values for POPC and POPC:bSM 1:4 are within ±1 nm of those shown for DOPC and DOPC:bSM 1:4, respectively. The data indicate that the outer leaflets of DOPCi/bSMo and POPCi/bSMo asymmetric SUVs are similarly ordered and both much closer to DOPC:bSM and POPC:bSM 4:1 mixtures than they are to pure disordered DOPC or POPC.

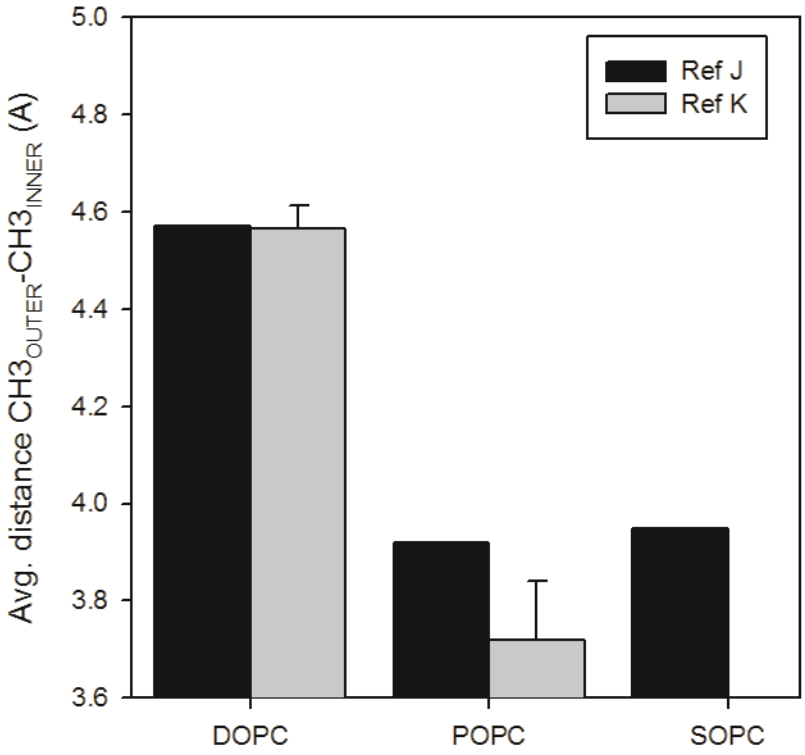

FIGURE S5. Methyl groups from opposing leaflets are closer in POPC and SOPC than in DOPC symmetric bilayers. Average distance between all the CH3 groups in one leaflet and the CH3 groups in the facing leaflet of symmetric DOPC, POPC or SOPC bilayers. The atomic coordinates were obtained from 400/500 ns molecular dynamics simulations at 293°K (8) (=Ref J) or averaged from the 2 snapshots of the last 2 ns of a simulation of 72 lipids at 303°K (9) (=Ref K). Error bars for the latter dataset represent average deviations.

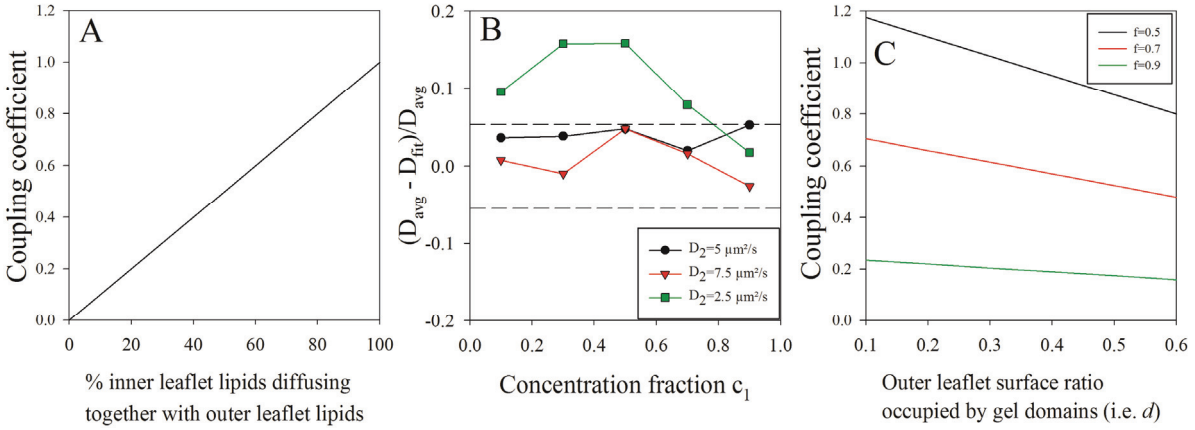

FIGURE S6. Interpretation of coupling coefficient. There are a number of possible interpretations of the coupling coefficient ($\Delta D_{inner}/\Delta D_{outer}$). The simplest is that it can be directly interpreted as a uniform decrease in D of all inner leaflet lipids due to a uniform decrease in D of all of the outer leaflet lipids. A variant of this can be derived if we assume that, in the inner leaflet of asymmetric GUVs, a fraction s of lipids diffuses as slow as the lipids in the outer leaflet (D_{inner} for fraction s is equal to D_{outer}) and the rest of the lipids (fraction 1-s) diffuses as fast as lipids in a symmetric GUV with composition comparable to the inner leaflet of the asymmetric GUVs (i.e. D_{inner} for fraction 1-s is equal to 10 µm²/s $\equiv D_{inner}^{fluid}$). Fitting the corresponding FCS curve with a one-component model (see below), would result in a measured diffusion coefficient for the inner leaflet

$$D_{inner} \approx s \times D_{outer} + (1 - s) \times 10 \frac{\mu m^2}{s} \qquad \text{(Eq.1)}$$

The resulting coupling coefficient would be

$$\text{coupling coefficient} = \frac{10^{\mu m^2/s} - D_{inner}}{10^{\mu m^2/s} - D_{outer}} = s \times \frac{10^{\mu m^2/s} - D_{outer}}{10^{\mu m^2/s} - D_{outer}} = s \qquad \text{(Eq. 2)}$$

Therefore, in this simple approximation, the coupling coefficient is equal to the fraction of lipids in the inner leaflet diffusing as slow as the lipids in the outer leaflet (panel A).

This raises the question: is it valid in this case to fit the FCS curve with one component? In the presence of two populations of diffusing molecules (e.g. with different diffusion coefficients D_1 and D_2), the FCS autocorrelation curve is determined by the diffusion times of each species. If such diffusion times (and therefore diffusion coefficients) are well separated, fitting of FCS data with a two-component diffusion model can provide the relative fraction of each population (i.e. c_1 and c_2, with $c_1+c_2=1$) and the corresponding diffusion coefficient. On the other hand, if the diffusion coefficients are not very different, a one-component model fit of a correlation curve corresponding to the diffusion of two species with different diffusion coefficients D_1 and D_2 could approximately result in a single D value which is the average of D_1 and D_2, weighted on the corresponding concentration fractions of the diffusing species. To verify whether this approximation could be applied to the typical diffusion coefficients we measured in our experiments, we calculated FCS autocorrelation curves, with D_1=10 µm²/s and using several values for D_2 and concentration fractions. Then, we analyzed these curves using a one-component diffusion model (thus obtaining a single D_{fit} value) and compared it to the average of D_1 and D_2, weighted on the respective concentration fractions (i.e. D_{avg}). Panel B shows the normalized differences between D_{fit} and D_{avg} as a

function of c_1 and for three different values of D_2. We found that the above-mentioned approximation is valid (with an error $\lesssim$5% of D_{avg}, see dashed lines in panel B) if D_1 =10 μm²/s and D_2 >5 μm²/s. These values are compatible with the maximum difference between D_{inner} and D_{outer} observed in our samples. Larger differences between D_1 and D_2 would result in a poor quality of the one-component fit and would, therefore, require the use of a two-component diffusion model.

An alternative interpretation of the coupling coefficient would be needed in the case that the outer leaflet of asymmetric GUVs has sub-microscopic gel domains (see main text). A mathematical description of random diffusion in such a situation is complex (10) but, since the probe we used to study diffusion (i.e. Atto-SM) has a low partition in ordered domains (2), we make the simplification of assuming that the above-mentioned domains are impenetrable obstacles to diffusion and that the lipids within them do not diffuse in the experimental time scale. In this regard, it is worth noting that typical reduction of D_{outer} that we measure (e.g relative D_{outer} of 60%) would require more than 60% of membrane surface to be occupied by gel phase, if the fluidity of the rest of the monolayer is not affected by the presence of SM (i.e. D~10 μm²/s) (10). Considering the concentration of SM in our samples and previous studies (11), gel domains that extensive are unlikely, and thus that the decrease in D in the outer leaflet is totally due to gel domain obstacles might also be unlikely. A more realistic alternative is that the decrease in D in the outer leaflet is due to a combination of gel domains acting as obstacles, some degree of fluorescent probe entry into the gel domains, with greatly slowed diffusion, and slower diffusion outside of gel domains due to the presence of some SM that is in the disordered regions of the membrane.

Nevertheless, if we assume the main factor decreasing diffusion in the outer leaflet is a significant presence of some gel domains that are impermeable round obstacles to lipid (and thus fluorescent probe) diffusion, under certain approximations,

$$D_{outer} = 10\,\frac{\mu m^2}{s} \times \frac{1-d}{1-0.6\times d} \qquad 0.1 < d < 0.6 \qquad \text{(Eq. 3)}$$

where d is the surface fraction of ordered domains (10).

In the case that the lateral distribution of lipids in the inner leaflet is not influenced by the presence of gel domains in the outer leaflet, a fraction d of inner leaflet lipids will be in spatial correspondence (i.e. in contact with across the bilayer midplane) with an outer leaflet gel domain. This lipid subset will transiently interact with outer leaflet lipids in the gel domains and therefore will be slowed by a factor f with respect to the diffusion in a symmetric fluid PC membrane

$$D_{inner}^{gel} = f \times D_{inner}^{liquid} = f \times 10\,\frac{\mu m^2}{s} \qquad \text{(Eq. 4)}$$

The resulting measured diffusion coefficient in the inner leaflet will be (similarly to Eq.1):

$$D_{inner} \approx d \times D_{inner}^{gel} + (1-d) \times D_{inner}^{fluid} \qquad \text{(Eq. 5)}$$

As mentioned above, this approximation for D_{inner} is valid for D_{inner}^{gel} values not too different from D_{inner}^{liquid}, i.e. 0.5< f <1

$$\text{coupling coefficent} = \frac{10^{\mu m^2/s} - D_{inner}}{10^{\mu m^2/s} - D_{outer}} = \frac{(1-f)\times d \cdot 10^{\mu m^2/s}}{10^{\mu m^2/s} - 10\frac{\mu m^2}{s} \times \frac{1-d}{1-0.6\cdot d}} = \frac{d\times(1-f)}{1-\frac{1-d}{1-0.6\times d}} \qquad \text{(Eq. 6)}$$

Panel C represents the calculated coupling coefficients according to Eq.6 as a function of *d* and for three values of *f*. Notice that it is possible in this model to obtain apparent coupling constants higher than 1. This is a consequence of the inner leaflet probes having more access to a low D compartment than the outer leaflet probes.

1. Kucherak, O. A., S. Oncul, Z. Darwich, D. A. Yushchenko, Y. Arntz, P. Didier, Y. Mely, and A. S. Klymchenko. 2010. Switchable nile red-based probe for cholesterol and lipid order at the outer leaflet of biomembranes. J. Am. Chem. Soc. 132: 4907-4916.
2. Sezgin, E., I. Levental, M. Grzybek, G. Schwarzmann, V. Mueller, A. Honigmann, V. N. Belov, C. Eggeling, U. Coskun, K. Simons, and P. Schwille. 2012. Partitioning, diffusion, and ligand binding of raft lipid analogs in model and cellular plasma membranes. Biochim. Biophys. Acta. 1818: 1777-1784.
3. Chiantia, S., P. Schwille, A. S. Klymchenko, and E. London. 2011. Asymmetric GUVs prepared by MbetaCD-mediated lipid exchange: an FCS study. Biophys. J. 100: L1-3.
4. Cheng, H. T., Megha, and E. London. 2009. Preparation and properties of asymmetric vesicles that mimic cell membranes: effect upon lipid raft formation and transmembrane helix orientation. J. Biol. Chem. 284: 6079-6092.
5. Chiantia, S., A. S. Klymchenko, and E. London. 2012. A novel leaflet-selective fluorescence labeling technique reveals differences between inner and outer leaflets at high bilayer curvature. Biochim. Biophys. Acta. 1818: 1284-1290.
6. Stockl, M., A. P. Plazzo, T. Korte, and A. Herrmann. 2008. Detection of lipid domains in model and cell membranes by fluorescence lifetime imaging microscopy of fluorescent lipid analogues. J. Biol. Chem. 283: 30828-30837.
7. Szabelski, M., D. Ilijev, P. Sarkar, R. Luchowski, Z. Gryczynski, P. Kapusta, R. Erdmann, and I. Gryczynski. 2009. Collisional quenching of erythrosine B as a potential reference dye for impulse response function evaluation. Applied spectroscopy. 63: 363-368.
8. Jambeck, J. P., and A. P. Lyubartsev. 2012. Derivation and systematic validation of a refined all-atom force field for phosphatidylcholine lipids. J. Phys. Chem. B. 116: 3164-3179.
9. Klauda, J. B., R. M. Venable, J. A. Freites, J. W. O'Connor, D. J. Tobias, C. Mondragon-Ramirez, I. Vorobyov, A. D. MacKerell, Jr., and R. W. Pastor. 2010. Update of the CHARMM all-atom additive force field for lipids: validation on six lipid types. J. Phys. Chem. B. 114: 7830-7843.
10. Wawrezinieck, L., H. Rigneault, D. Marguet, and P. F. Lenne. 2005. Fluorescence correlation spectroscopy diffusion laws to probe the submicron cell membrane organization. Biophys. J. 89: 4029-4042.
11. Ahmed, S. N., D. A. Brown, and E. London. 1997. On the origin of sphingolipid/cholesterol-rich detergent-insoluble cell membranes: physiological concentrations of cholesterol and sphingolipid induce formation of a detergent-insoluble, liquid-ordered lipid phase in model membranes. Biochemistry. 36: 10944-10953.